Water Research 245 (2023) 120589

Contents lists available at ScienceDirect

Water Research

journal homepage: www.elsevier.com/locate/watres

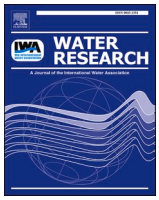

Impact of redox fluctuations on microbe-mediated elemental sulfur disproportionation and coupled redox cycling of iron

Ke Zhang [a,b,1], Shaojian Zhang [b,1], Peng Liao [b,*], Yuanxin Zhao [b], Min Gan [a], Jianyu Zhu [a,*]

[a] School of Minerals Processing and Bioengineering, Key Laboratory of Biohydrometallurgy of Ministry of Education, Central South University, Changsha 410083, PR China

[b] State Key Laboratory of Environmental Geochemistry, Institute of Geochemistry, Chinese Academy of Sciences, Guiyang 550081, PR China

ARTICLE INFO

Keywords:
Elemental sulfur
Microbial respiration
Sulfur cycling
Iron transformation
Redox fluctuation

ABSTRACT

Elemental sulfur (S^0) plays a vital role in the coupled cycling of sulfur and iron, which in turn affects the transformation of carbon and various pollutants. These processes have been well characterized under static anoxic or oxic conditions, however, how the natural redox fluctuations affect the bio-mediated sulfur cycling and coupled iron cycling remain enigmatic. The present work examined S^0 disproportionation as driven by natural microbial communities under fluctuating redox conditions and the contribution of S^0 disproportionation to ferrihydrite transformation. Samples were incubated at either neutral or alkaline pH values, applying sequential anaerobic, aerobic and anaerobic conditions over 60 days. Under anaerobic conditions, S^0 was found to undergo disproportionation to sulfate and sulfide, which subsequently reduced ferrihydrite at both pH 7.4 and 9.5. Ferrihydrite promoted S^0 disproportionation by scavenging biogenic sulfide and maintaining a suitable degree of sulfate formation. After an oxic period, during the subsequent anoxic incubation, bioreduction of sulfate occurred and the biogenic sulfide reduced iron (hydr)oxides at a rate approximately 25 % lower than that observed during the former anoxic period. A 16S rDNA-based microbial community analysis revealed changes in the microbial community in response to the redox fluctuations, implying an intimate association with the coupled cycling of sulfur and iron. Microscopic and spectroscopic analyses confirmed the S^0-mediated transformation of ferrihydrite to crystalline iron (hydr)oxide minerals such as lepidocrocite and magnetite and the formation of iron sulfides precipitated under fluctuating redox conditions. Finally, a reaction mechanism based on mass balance was proposed, demonstrating that bio-mediated sulfur transformation maintained a sustainable redox reaction with iron (hydr)oxides under fluctuating anaerobic-aerobic-anaerobic conditions tested in this study. Altogether, the finding of our study is critical for obtaining a more complete understanding of the dynamics of iron redox reactions and pollutant transformation in sulfur-rich aquatic environments.

1. Introduction

Sulfur is a redox-active element that occurs in most aquatic environments and can drive a spectrum of redox reactions that govern the redox cycling of sulfur, iron, carbon, and pollutants in natural and engineered systems (Kappler et al., 2021; Milucka et al., 2012). The redox state of sulfur ranges from +6 to –2, allowing for interconversions among different sulfur species *via* microbial activity and chemical reactions. Sulfur species with intermediate redox states, including elemental sulfur (S^0), polysulfides, and thiosulfate, can be readily metabolized by certain organisms (e.g. *Db. Propionicus* and *Desulfurivibrio alkaliphilus*) and may serve as important sources of energy (Dahl and Friedrich, 2008; Philippot et al., 2007). Furthermore, the redox reactions of sulfur species with environmental compounds, such as iron (hydr)oxides and organic matter (Peiffer et al., 1992; Yu et al., 2015; Wang et al., 2023a), contribute to redox reactions that can control the transformations of various pollutants such as heavy metals (e.g., Hg, As, Cr, Sb), organic pollutants (e.g., nitro compounds and halogenated compounds), and nutrients (e.g., NO_3^{3-}, PO_4^{3-}), *via* adsorption, incorporation, and redox reactions (Bai et al., 2023; Borch et al., 2010; He et al., 2023; Karimian et al., 2018; Qiu et al., 2020; Wang et al., 2022; Zhang et al., 2022; Zou et al., 2023), thus maintaining specific ecosystems.

* Corresponding authors.
E-mail addresses: liaopeng@mail.gyig.ac.cn (P. Liao), zhujy@csu.edu.cn (J. Zhu).
[1] These authors contributed equally.

https://doi.org/10.1016/j.watres.2023.120589
Received 25 April 2023; Received in revised form 4 September 2023; Accepted 5 September 2023
Available online 10 September 2023

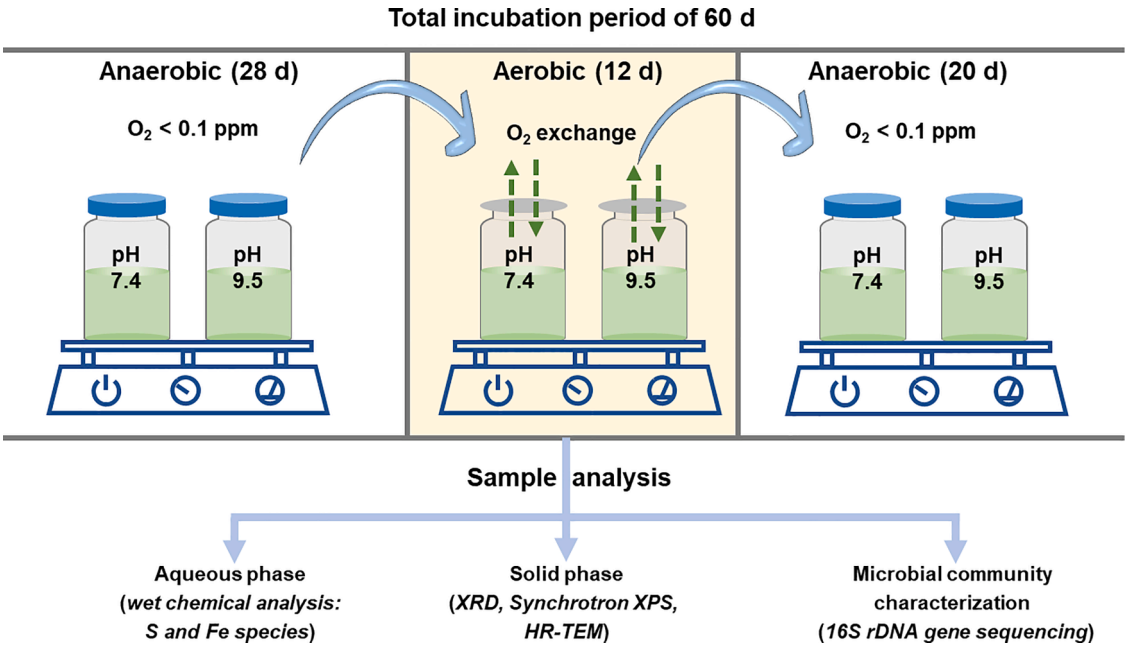

Fig. 1. The experimental design of this study.

As a major sulfur species with intermediate redox state, S^0 is commonly found in terrestrial hot springs as well as marine and freshwater sediments, and can act as either an electron donor or acceptor in various sulfur-mediated geochemical processes (Karimian et al., 2018; Thamdrup et al., 1993). Given the abundant occurrence of S^0 in aquatic systems, with concentration ranging from several to hundreds μg g^{-1} (Burton et al., 2006; Troelsen and Jørgensen, 1982; Wang et al., 2023b; Yücel et al., 2010), S^0-mediated electron transfer processes are likely to play an important role in the transformation of elements and pollutants in aquatic environments. Disproportionation of S^0 to sulfide and sulfate is a critical part of sulfur cycling, affecting the cycling of iron and carbon (Flynn et al., 2014; Thamdrup et al., 1993). Furthermore, iron (hydr) oxides have been found to promote the disproportionation of S^0 by reacting with generated sulfide (Finster, 2008; Thamdrup et al., 1993). Recent advances have also revealed that iron (hydr)oxides can, in turn, promote rapid microbial sulfate reduction by stimulating cryptic sulfur cycling under anoxic conditions (Hansel et al., 2015; Jørgensen et al., 2019). However, previous studies investigating the coupled cycling of sulfur and iron focused heavily on either anoxic or oxic conditions (Bronner et al., 2023; Flynn et al., 2014; Poser et al., 2013). These single condition studies fail to accurately represent the natural, redox dynamic conditions, where the coupled cycling of sulfur and iron under fluctuating redox conditions is also of prime importance.

In many subsurface environments (e.g., coastal sediments, floodplain/wetlands soils, shallow aquifer sediments), the water table undergoes periodic fluctuations between oxic surface water and anoxic groundwater. The fluctuation create a zone with redox fluctuations (Karimian et al., 2018; O'Day et al., 2004; Peiffer et al., 2021; Sharma et al., 2022; Zhao et al., 2022). When O_2-containing rainfall and surface water infiltrate this zone, a temporary influx of O_2 promotes the chemical oxidation of Fe(II) and sulfide. Conversely, when anoxic aquifer water diffuses upward or O_2 is depleted, previously formed oxidized iron and sulfur species (i.e., Fe(III) (hydr)oxides and sulfate) can be reduced (Thompson et al., 2006). Therefore, the biogeochemical cycling of sulfur and iron frequently occurs within these fluctuating redox environments, characterized by active sulfur and iron compounds interacting with diverse microbial communities (Ginn et al., 2017; Zhang et al., 2020). Thus, it is reasonable to assume that redox fluctuations would play a significant role in the interplay between S^0, iron, and bacteria, thereby influencing element cycling and pollutant transformation. However, our understanding of the role of S^0 in iron cycling and the reciprocal effect of iron in sulfur cycling under fluctuating redox conditions is still limited. Particularly, it remains enigmatic whether sustainable electron transfer reactions can be maintained during anoxic conditions after an oxic period. Therefore, it is crucial to develop a mechanistic and quantitative understanding of the role of redox fluctuations in S^0-mediated cycling of sulfur and iron. Such information is essential for comprehensively understanding the iron-sulfur reaction framework and accurately assessing pollutant mitigation processes.

The objective of the present study was to assess the impact of redox fluctuations on bio-mediated S^0 disproportionation in conjunction with the transformation of iron (hydr)oxides over a range of environmentally relevant conditions. To this end, laboratory microcosms mimicking the S^0 disproportionation occurring in natural microbial communities were employed. To better represent fluctuating redox conditions, the experimental microbial communities were obtained from a lake sediment and incubated at both neutral and alkaline pH values *via* a sequential anaerobic-aerobic-anaerobic process over a 60 d time span. Throughout the experimental work, various sulfur and iron species in addition to the microbial communities were periodically analyzed using a combination of aqueous and solid phase techniques. Results gained from this study are expected to greatly expand our understanding of the role of S^0 in sulfur cycling and the redox-based transformation of iron under fluctuating redox conditions. This work will also provide increased knowledge concerning the S^0-mediated transformation of pollutants in sulfur-rich aquatic environments.

2. Materials and methods

2.1. Microbes and materials

All chemicals were purchased from Sinopharm Chemical Reagent Co., Ltd. and were of analytical grade. The cultivation medium, bacterial community, and cultivation conditions are described in detailed in Text S1 of the Supplementary Materials (SM). Briefly, cultivation medium was prepared and autoclaved at 120 ± 2 °C for 20 min. After cooling to room temperature, the medium was transferred into an anoxic glovebox filled with a mixture of 5 % H_2 and 95 % N_2 (O_2 < 0.1 mg/L, COY Laboratory, with Pd catalyst). The native microbial community was

obtained from a lake sediment in Southwest China (Fig. S1), which was collected at a depth of 30 m below ground surface. The powdered elemental sulfur (Sinopharm Chemical Reagent Co., Ltd) used in this work was stored overnight in the anoxic glovebox to remove adsorbed O_2. Ferrihydrite was synthesized following Schwertmann and Cornell (2008) (see details in Text S2).

2.2. Batch incubations

All batch experiments were performed at least in duplicate. Trials involving the biotransformation of S^0 were carried out in 250 mL serum bottles containing 150 mL culture medium in the absence or presence of ferrihydrite. In the case of incubation in the absence of ferrihydrite, approximately 45 mg of powdered S^0 was transferred into the bottle to yield an initial S° concentration of 9.38 mM. In the trials incorporating ferrihydrite, both ferrihydrite and S^0 were added so as to obtain concentrations of 9.38 mM Fe(III) and 3.12 mM S^0. A control batch was also produced containing ferrihydrite at the level of 9.38 mM Fe(III) but without S^0. Prior to each incubation, 12 mM of sodium acetate was added as a carbon source for bacterial growth, after which the enriched bacterial strain was inoculated into the incubation medium to give an initial bacterial concentration of approximately 1×10^8 cells/mL and to initiate the reaction. To explore the effect of pH on the dissimilatory metabolisms of S^0 and ferrihydrite, incubations were performed at pH values of 7.4 or 9.5, based on the pH values typically found in natural waters and alkaline aquifers, respectively (Flynn et al., 2014; Poser et al., 2013). The pH values were buffered using 0.030 g/L KH_2PO_4 contained in culture medium by adding 0.1 M HCl or 0.1 M NaOH solution to desired pH values following Bingjie et al. (2014) and Shi et al. (2020). All incubations involved successive anaerobic (28 d), aerobic (12 d), and anaerobic (20 d) periods over a total span of 60 d (see Fig. 1 for the experimental design). Each incubations vial was initially prepared in the anoxic glovebox then crimp-sealed with a rubber stopper and aluminum cap to ensure anaerobic conditions inside the vial (the dissolved oxygen concentration was < 0.1 mg/L), following which the vial was incubated at 30 ± 2 °C while agitated using a horizontal shaker (180 rpm) for 28 d under anaerobic conditions. This incubation temperature was selected because the optimum growth for sulfur-metabolism bacteria is at 28–32 °C (El Houari et al. 2017; Kojima et al., 2016; Shimoshige et al., 2022). To strengthen the agitation, a 4 cm-long glass bar was placed in the reaction vial. After the first anaerobic incubation, the incubations vials were transferred to aerobic conditions, where the rubber stopers and aluminum caps were replaced with 0.22 μm pore-size breathable sealing films. This operation allows an air exchange between the vial headspace and the atmosphere ($P_{O2} = 0.21$ bar) to initiate the aerobic incubation. We monitored the dissolved O_2 concentration in the suspension and observed that after 6 h the dissolved O_2 concentration reached a level greater than 6.3 mg/L, indicating that the reaction suspensions were well oxygenated. For the second anaerobic incubation, the vials were purged with 99.99 % N_2 for 0.5 h to remove dissolved oxygen then transferred into the anaerobic condition again. The vials were subsequently sealed with rubber stoppers and aluminum caps and incubated on a horizontal shaker for a further 20 d. In addition to biotic experiments, abiotic controls (no bacteria addition) were performed with 3.12 mM S^0 and 9.38 mM Fe(III) ferrihydrite under anoxic conditions at pH 7.4 and 9.5, respectively. After 60 d of reaction, no reaction products such as Fe(II) (< 1.8 μM), S(-II) (< 2.5 μM), and SO_4^{2-} (< 1.1 μM) were detected (Fig. S2), indicating that the abiotic reaction between S^0 and ferrihydrite can be excluded in our study.

The sulfur species having intermediate redox states, such as polysulfides and thiosulfates, that are likely to be produced during sulfur cycling are reactive and tend to disproportionate to generate sulfate (Jørgensen, 1990a, 1990b; Poser et al., 2013). Therefore, to assess the effects of polysulfides and thiosulfate on sulfate formation, a complementary experiment was performed under anaerobic conditions (see Text S3). In addition, sulfate (a potential S^0 transformation product) may affect the biotransformation of S^0. Thus, another complementary incubation incorporating sulfate but not ferrihydrite was conducted to assess the effect of sulfate on the biotransformation of S^0 (see Text S4). Considering that the S° concentration in natural environments spans a wide range from several to hundreds of μg g^{-1} (Burton et al., 2006; Yücel et al., 2010), this work additionally examined the effect of S° concentration on the transformation of S^0 at a fixed ferrihydrite concentration of 9.38 mM Fe(III). In these trials, the S/Fe molar ratio was set to 1:9, 1:6, and 1:1 with S° concentrations of 1.03, 1.56, and 9.38 mM, respectively. The incubation conditions and procedures were the same as those applied during the incubation experiments with a fixed S° concentration of 3.12 mM.

2.3. Analytical methods

Subsamples were collected periodically during each anaerobic and aerobic period for wet chemistry analysis, solids characterization, and microbial community analysis. To minimize any effect of O_2, O_2-sensitive samples were promptly processed under anaerobic conditions.

2.3.1. Wet chemical analysis

Elemental sulfur remaining in each suspension was first extracted by dissolving a 0.1 mL aliquot of the unfiltered suspension in 1 mL of oxygen-free methanol. After shaking for 20 min, the sample was passed through a 0.22 μm poly(tetrafluoroethylene) syringe filter and the resulting filtrate was analyzed by high performance liquid chromatography (HPLC, Agilent 1290 Infinity) with ultraviolet/visible (UV/VIS) Diode Array detection following Wan et al. (2014). The HPLC instrument was equipped with a reverse phase C18 column and a methanol/water mixture (95 % methanol) was used as the eluent. The sulfide concentration in the aqueous phase (< 0.22 μm) was determined using the methylene blue method (Cline, 1969). The concentration of sulfide that associated with iron (referred to as acid volatile sulfide, AVS) was determined by mixing a 0.2 mL of suspension with 0.2 mL of anoxic 12 M HCl in a serum bottle containing a sulfide trap comprising 0.15 mL of 10 wt% zinc acetate solution and incubated for 24 h. The trapped sulfide was quantified using the methylene blue method. The concentration of aqueous polysulfides (S_n^{2-}, $2 \leq n \leq 8$) (< 0.22 μm) was photometrically determined at 285 nm (see details in Text S5) (Kleinjan et al., 2005). The sulfate and thiosulfate concentrations were determined by analyzing aqueous samples using ion chromatography (ICS90, Dionex) with a $NaHCO_3/Na_2CO_3$ solution as the eluent following Hansel et al. (2015). Total Fe(II) ($Fe(II)_{tot}$) was determined after digesting a 0.5 mL unfiltered aliquot with 0.1 mL of 6 M HCl for 12 h at room temperature in the dark. A desired amount of fluoride was added to inhibit the formation of colored Fe(III)-phenanthroline complexes (Liao et al., 2017; Tamura et al., 1974). The resulting suspension was centrifuged and the supernatant was analyzed using the 1,10-phenanthroline method (Tamura et al., 1974).

2.3.2. Microscopic and spectroscopic analyses of solid phase species

Solid samples were collected at the end of the corresponding anaerobic/aerobic incubation periods by centrifugation, freeze-dried, and then stored in an anaerobic glovebox for further characterization using X-ray diffraction (XRD), high-resolution transmission electron microscopy (HR-TEM), and synchrotron-based X-ray photoelectron spectroscopy (XPS). The phase transformation of the ferrihydrite was monitored by XRD using a Rigaku MiniFlex X-ray diffractometer with Ni-filtered Cu Ka radiation in angles ranging from 10° to 90° 2θ in 0.02° steps and employing the MDI JADE 6 software package. The morphologies of the solid particles were characterized based on TEM observations with a JEM-2100 instrument operating at 200 keV (LaB6, JEOL Ltd., Japan) in conjunction with selected-area electron diffraction (SAED). Changes in the oxidation states of sulfur and iron were characterized by XPS performed at the Catalysis and Surface Science

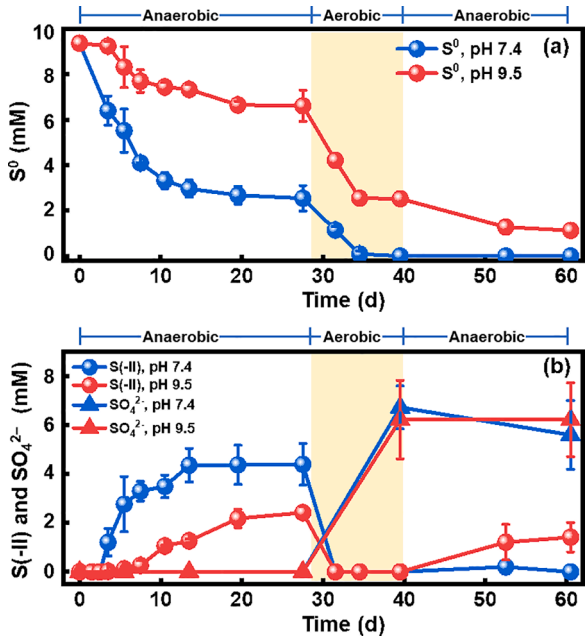

Fig. 2. Evolutions of (a) S^0 and (b) S(-II) and SO_4^{2-} in the incubations of S^0 without ferrihydrite at 30 ± 2 °C. The incubations went through an anaerobic period in the first 28 d, followed by an aerobic period for 12 d (shaded area), and then a 20-d anaerobic period again. The variation in pH was < 0.3 pH unit throughout the whole incubation period. Error bars represent the standard deviations of at least duplicate measurements. Where error bars are not visible, they are smaller than the data symbols.

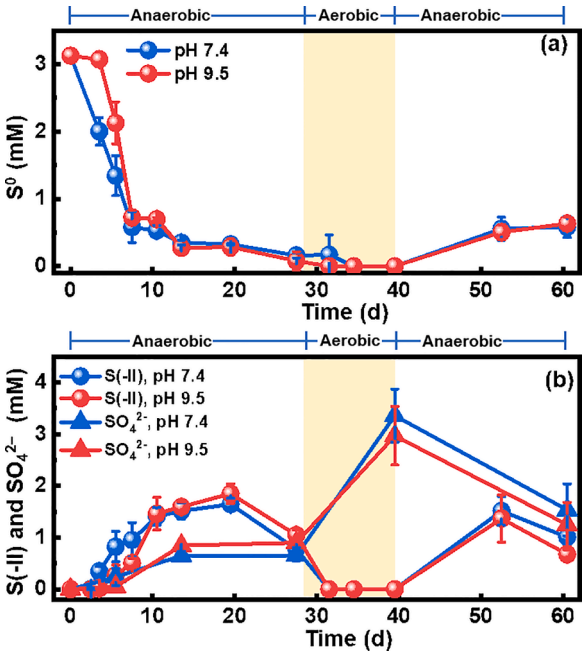

Fig. 3. Evolutions of (a) S^0 and (b) S(-II) and SO_4^{2-} in the incubations of S^0 amended with ferrihydrite (9.38 mM Fe) at 30 ± 2 °C. The incubations went through an anaerobic period in the first 28 d, followed by an aerobic period for 12 d (shaded area), and then a 20-d anaerobic period. The variation in pH was < 0.3 pH unit throughout the whole incubation period. Error bars represent the standard deviations of at least duplicate measurements. Where error bars are not visible, they are smaller than the data symbols.

Endstation at the BL11U beamline in the National Synchrotron Radiation Laboratory (NSRL) in Hefei, China (see details in Text S6). To obtain the vertical distribution of Fe and S along the surface of sample, a fine-scale XPS depth profiling technique was used to etch samples from sample top-surface to a depth of approximately 20 nm using an argon gun operating at 2 kV over a duration of 20 min (Li et al., 2022; Zhu et al., 2014). C 1s and Fe 2p spectra were obtained on the monochromatic Al *Ka* X-ray source while S 2p spectra were acquired using a synchrotron beam at 380 eV. The binding energy data obtained from the synchrotron beam were calibrated using the bulk Au $4f_{7/2}$ core level located at 84.0 eV following Ding et al. (2020). In the case of data acquired using the Alka beam, the binding energies were calibrated relative to the C 1s peak at 284.8 eV as an internal standard. Peak-fitting was performed *via* a least squares procedure with the Gaussian-Lorentzian function (80 % Gaussian-20 % Lorentzian) after subtracting a Shirley background, using the CasaXPS 2.3.16 software package.

2.3.3. Microbial community

The evolutions of microbial communities were investigated by taking suspension aliquots in triplicate at regular intervals for high-throughput sequencing of the 16S rDNA gene. The bacterial primers for sequencing were 338 F (5′-ACTCCTACGGGAGGCAGCA-3′) and 806R (5′-GGACTAHVGGGTWTCTAAT-3′). Raw sequencing reads were quality trimmed using the Quantitative Insights Into Microbial Ecology (QIIME 1.8.0) program. Tags were clustered with 97 % similarity by employing the Usearch software and taxonomic annotations were analyzed based on Silva (bacteria) taxonomic databases. The 16S rDNA sequence data were analyzed using the PICRUSt genome prediction software to assess the functional gene compositions in the samples. Data are presented herein in the form of mean ± standard deviation. The statistical significance of differences between samples was determined using the one-way analysis of variance (ANOVA) technique followed by Duncan's multiple range test in the SPSS 22.0 software package and a p value < 0.05 was considered statistically significant.

3. Results and discussion

3.1. Biotransformation of S^0 in the absence of ferrihydrite

During the first anaerobic incubation of the trial without ferrihydrite, S^0 was consumed while S(-II) was generated but SO_4^{2-} was not detected (Fig. 2). Furthermore, the biotransformation of S^0 at pH 7.4 was more rapid than at pH 9.5. After 14 d of incubation, the S° concentration decreased from an initial value of 9.38 mM to 2.96 mM at pH 7.4 and to 7.34 mM at pH 9.5 (Fig. 2a), with the simultaneous formation of S(-II) to give concentrations of 4.36 and 1.27 mM at these same pH values, respectively (Fig. 2b). This observation contradicts the observation made by Flynn et al. (2014) that the reduction of S^0 is more favorable at higher pH values. This discrepancy can possibly be explained by higher bacterial activity at pH 7.4 based on the bacterial community having been obtained from a near-neutral lake sediment (Hao et al., 1996).

During the subsequent aerobic incubation, both S^0 and S(-II) were quickly consumed in conjunction with the rapid formation of sulfate. In contrast, during the second anaerobic incubation, the sulfate concentration remained almost unchanged while the sulfide concentration accumulated, reaching levels below 0.2 mM at pH 7.4 and 1.4 mM at pH 9.5 (Fig. 2b). Clearly, during anaerobic incubations, sulfur-reducing bacteria in the suspension reduced S^0 to S(-II) (see microbial community analysis in the section of *Microbial community dynamics*) (Eq. (1)). In addition, under aerobic conditions, S^0 and S(-II) were both oxidized by reaction with O_2 to form SO_4^{2-} (Eq. (2)). Given that the sulfur-reducing bacteria were also able to reduce sulfate to S(-II) (Eq. (3)), therefore, the evident lack of sulfate during the first anaerobic incubation does not guarantee that sulfate was not produced. These data demonstrate that the bioreduction of S^0 occurred and the formation of sulfate is significantly restrained in the absence of ferrihydrite, and the extent of reduction is more pronounced at neutral pH compared to alkaline pH.

$$S^0 + CH_2O_{org} + 2H_2O \xrightarrow{\text{microbial}} H_2S + HCO_3 + H^+ \quad (1)$$

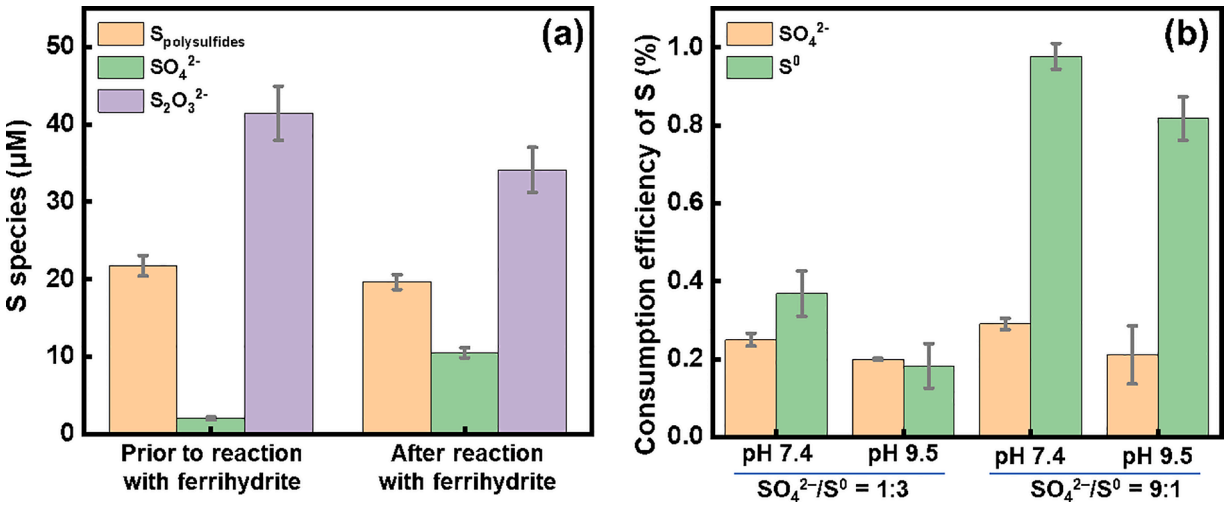

Fig. 4. (a) Complementary experiments of the effect of polysulfides and thiosulfate on the formation of sulfate in the presence of ferrihydrite (1 g/L) at 30 ± 2 °C and pH 9.5 under anaerobic conditions. The dataset labelled with prior to reaction with ferrihydrite was obtained from the incubation of MR-1+S^0 without ferrihydrite after 6 d of reaction, and the dataset labelled with after reaction with ferrihydrite was obtained from the incubation of MR-1+S^0 with ferrihydrite amendment after 4 d of reaction (see Text S3). (b) Complementary experiments of the effect of sulfate on biotransformation of S^0 in the absence of ferrihydrite under anoxic conditions at 30 ± 2 °C. The consumption efficiencies of sulfate and S^0 were calculated by dividing the consumed concentration by the initial concentration. Error bars represent the standard deviations of at least duplicate measurements.

$$S(-II) \overset{O_2}{\rightarrow} S^0 \overset{O_2}{\rightarrow} SO_4^{2-} \quad (2)$$

$$SO_4^{2-} + 2CH_2O_{org} \overset{microbial}{\rightarrow} H_2S + 2HCO_3 \quad (3)$$

3.2. *Biotransformation of S^0 in the presence of ferrihydrite*

3.2.1. *Evolution of sulfur species with ferrihydrite*

Ferrihydrite addition stimulated the disproportion of S^0 to sulfide and sulfate during the first anaerobic incubation (Fig. 3). At both pH 7.4 and 9.5, the S° concentration decreased rapidly from the initial value of 3.12 mM to 0.27–0.35 mM after 14 d and then to 0.08–0.16 mM by the end of the incubation (i.e., after 28 d) (Fig. 3a). Simultaneously, after 14 d of incubation, the sulfide and sulfate concentrations were increased to 1.51–1.59 and 0.65–0.85 mM, respectively (Fig. 3b). The ratio of the moles sulfide generated to the moles sulfate generated was in the range of 1.8 to 2.3 and so was lower than the expected value of 3 based on Eq. (4) (Poser et al., 2013; Thamdrup et al., 1993). This discrepancy can likely be attributed to the oxidation of sulfide by the ferrihydrite (Eq. (5)). As a result, a general stoichiometry for the turnover can be expressed by Eq. (6). The variable x, which represents the fraction of generated sulfide from Eq. (4) and its subsequent reaction with iron (hydr)oxides as described in Eq. (5), will be discussed and estimated in the following section.

$$4S^0 + 4H_2O \rightarrow SO_4^{2-} + 3HS^- + 5H^+ \quad (4)$$

$$3H_2S + 2FeOOH \rightarrow S^0 + 2FeS + 4H_2O \quad (5)$$

$$(4-x) * S^0 + 2x * FeOOH + 4 * (1-x) * H_2O \rightarrow SO_4^{2-} + 3(1-x) * HS^- + 2x * FeS + (5-3x) * H^+ \quad (6)$$

In addition, a decrease in the sulfide concentration was observed at the end of the first anaerobic period (over the time span of 20–28 d). This finding is consistent with the decrease in the total Fe(II) concentration (cf. Fig. 6), indicating a reaction between FeS and Fe(II) as previously reported by Hellige et al. (2012) that FeS, S^0, and Fe(II) reacted to produce FeS_2 and Fe_3O_4 (Eq. (7)).

$$S^0 + FeS + Fe(II) + 2FeOOH \rightarrow FeS_2 + Fe_3O_4 + 2H^+ \quad (7)$$

During the aerobic period, both S^0 and sulfide were oxidized by O_2 to sulfate, which is similar to the results obtained from incubation in the absence of ferrihydrite (Eq. (1)). The peak sulfate concentration was 2.96–3.36 mM and so was approximately equal to the initial S^0 level of 3.12 mM. During the second anaerobic incubation (40–60 d), S^0 and S (-II) again accumulated (Fig. 3) in conjunction with the generation of Fe(II) (cf. Fig. 6). This regeneration of S° can likely be ascribed to the oxidation of sulfide by Fe(III)-based minerals (Eq. (5)). This phenomenon suggests that bio-mediated sulfur cycling still occurred after 60 d of anaerobic-aerobic-anaerobic fluctuations.

It is worth noting that sulfate was always present under the anaerobic conditions. Sulfate concentrations in the range of 0.65–0.85 mM were found during the first anaerobic incubation (Fig. 3b). Among the various pathways contributing to sulfate formation, the disproportionation of S^0 to SO_4^{2-} and S^{2-} is important (Eq. (4)) (Thamdrup et al., 1993). Furthermore, ferrihydrite is able to scavenge the generated sulfide, thus promoting the disproportionation of S^0 (Finster, 2008; Thamdrup et al., 1993). On this basis, it appears that the formation of sulfate under anaerobic conditions is maintained by sulfur cycling in the presence of ferrihydrite.

As noted, a complementary experiment was performed to examine the effects of polysulfides and thiosulfate on sulfate formation (see Text S3). During this trial, the biogenic sulfide was found to be consumed through reaction with introduced ferrihydrite, accompanied with the formation of Fe(II) and FeS (Fig. 4a and Table S1). The polysulfides concentration was found to remain constant over the first 4 d In contrast, the thiosulfate concentration decreased by approximately 12.8 μM, while the sulfate concentration increased by approximately 10.1 μM (Fig. 4a and Table S1). These observations suggest that the ferrihydrite reacted with thiosulfate, rather than polysulfides, to produce sulfate (Eq. (8)). Our findings align with the observations made by Wan et al. (2014) regarding the interaction between iron (hydr)oxides (goethite and lepidocrocite) and aqueous sulfide. Wan et al. (2014) noted the presence of polysulfides but not sulfate during this interaction, suggesting that the reaction of polysulfides with iron (hydr)oxides does not lead to the generation of sulfate. Although thiosulfate was not detected during the anaerobic-aerobic-anaerobic incubation, the formation of this species cannot be excluded because any thiosulfate that was produced may have been consumed by reaction with iron (hydr)oxides (Eq. (8)) or microbial respiration (Eq. (9)) (Jørgensen, 1990a, 1990b), thus

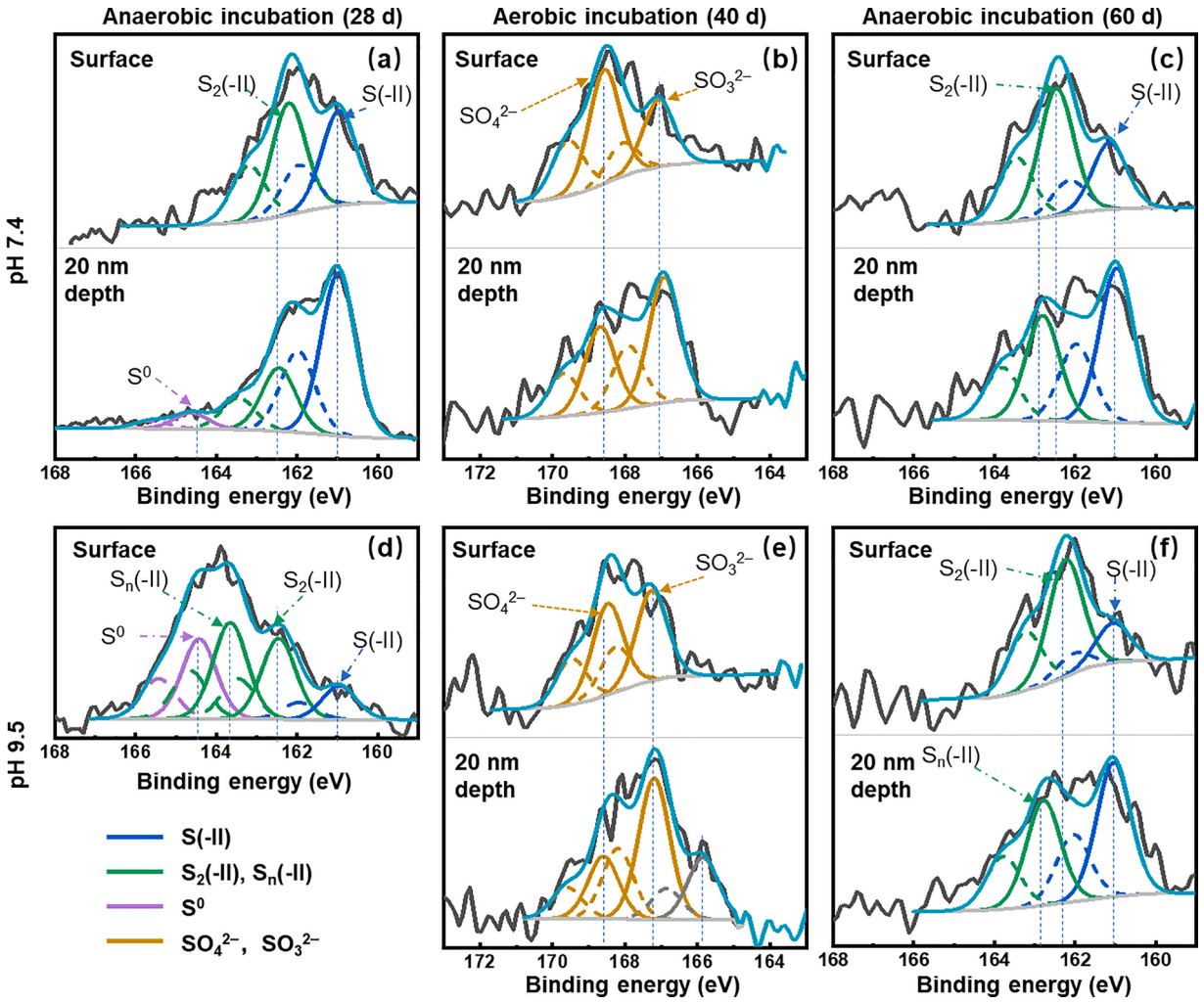

Fig. 5. Synchrotron XPS S 2p spectra of solid samples collected (a,d) at the end of first anaerobic incubation (28 d), (b,e) at the end of aerobic incubation (40 d), and (c,f) at the end of second anaerobic incubation (60 d). Spectra of (a–c) are samples collected at pH 7.4, and spectra of (d–f) are samples collected at pH 9.5. The probing depths were recorded at the surface and approximately 20 nm depth along the sample surface. Each S 2p spectrum was fitted with a doublet due to spin-orbit splitting of S 2 $p_{1/2}$ (dashed line) and S $2p_{3/2}$ (solid line). Peak fitting for S 2p peaks was assigned based on literature-reported values summarized by Baraket et al. (2007), Nandasiri et al. (2017) and Wan et al. (2014).

contributing to sulfate formation. Moreover, the complementary experiment intended to examine the effect of sulfate on the biotransformation of S^0 (see Text S4) demonstrated that both sulfate and S^0 were consumed at pH values of 7.4 and 9.5 (Fig. 4b). These results suggest that, under anaerobic conditions, considerable S^0 bioreduction can occur even in the presence of sulfate. These data provide further evidence for the important role of S^0 in sulfur cycling.

$$S_2O_3^{2-} + 8FeOOH + 14H^+ \rightarrow 2SO_4^{2-} + 8Fe^{2+} + 11H_2O \quad (8)$$

$$S_2O_3^{2-} + H_2O \xrightarrow{microbial} SO_4^{2-} + HS^- + H^+ \quad (9)$$

The biotransformation of S^0 in the presence of ferrihydrite was investigated using synchrotron-based XPS combined with a depth profiling technique. At the end of both anaerobic incubation periods (i.e., after 28 and 60 d), these analyses established that reduced sulfur species (meaning S(-II) (161.2 ± 0.3 eV), S_2(-II) (162.1 ± 0.2 eV) and S_n(-II) ($n > 2$) (163.2 ± 0.3 eV)) were the main sulfur species (Fig. 5a, c, d and f). The samples collected after 28 d each generated a characteristic S^0 peak at 164.5 eV, consistent with the results of the wet chemical analysis showing that traces of S^0 remained in the suspensions. Despite the observation of the S^0 peak, its precise determination was challenging due to the volatilization of S^0 under ultrahigh vacuum of the XPS (i.e., 1.0×10^{-8} Torr) (Hampton et al., 2011). Further cryogenic XPS analysis is required to prevent volatilization and improve the intensity of the S^0 peak measurement (Wan et al., 2014). The XPS depth profiling results showed that more intense disulfide/polysulfide peaks were obtained at the near-surface (i.e., typically the topmost 1 − 10 nm) compared with a depth of approximately 20 nm along the surface. In contrast, the intensity of the S(-II) peak was higher at a depth of approximately 20 nm along the surface (Fig. 5a, c and f). This observation implies that the residual S^0 might have been associated with the reaction of sulfide to produce disulfide and polysulfides at the near-surface of iron minerals. In contrast to the wet chemistry results, sulfate was not detected by XPS, possibly because the sulfate concentrations were low in the solid samples. However, following aerobic incubation for 12 d (at 40 d), characteristic peaks of sulfate (at 168.6–169.2 eV) and sulfite (at approximately 167.2 eV) (Baraket et al., 2007; Nandasiri et al., 2017; Wan et al., 2014) appeared at both pH 7.4 and 9.5, accompanied by the disappearance of the sulfide peaks (Fig. 5b and e). Evidently, after an oxic period, active sulfate reduction and sulfide generation occur once subject in a subsequent anaerobic incubation, thereby driving continued iron redox transformations.

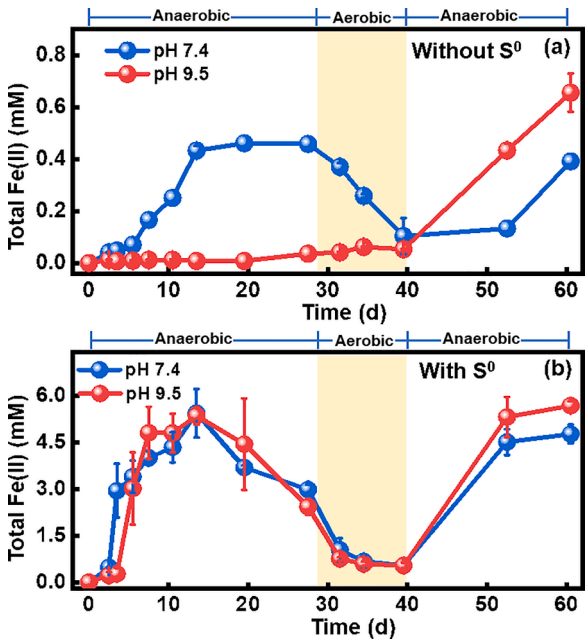

Fig. 6. Evolution of Fe(II) in the incubations (a) without S^0 amendment and (b) with S^0 amendment at 30 ± 2 °C. The incubations went through an anaerobic period in the first 28 d, followed by an aerobic period for 12 d (shaded area), and then an anaerobic period for 20 d. The variation in pH was < 0.3 pH unit throughout the whole incubation period. Error bars represent the standard deviations of at least duplicate measurements. Where error bars are not visible, they are smaller than the data symbols.

3.2.2. *Biotransformation of S^0 in conjunction with the reduction of ferrihydrite*

The biogenic sulfide from S^0 greatly promoted ferrihydrite reduction under the anaerobic conditions. During the first anaerobic incubation (0–28 d) without the addition of S^0, the Fe(II) concentration was below 0.5 mM at pH 7.4 and below 0.1 mM at pH 9.5 (Fig. 6a). In comparison, with S^0 at both pH 7.4 and 9.5, the $Fe(II)_{tot}$ concentration was in the range of 5.35–5.44 mM after 14 d, accounting for 57 % of total Fe (Fig. 6b). Therefore, compared to the sulfur-mediated Fe(III) reduction, the dissimilatory Fe(III) reduction is of minor significance. Given the strong coupling between the disproportionation of S^0 and Fe(III) reduction, we can estimate the extent of interaction between biogenic sulfide and iron (hydr)oxides, represented as the variable x in Eq. (6). Based on the mole ratios of Fe(II) to sulfide collected at 14 d, x is calculated to be 1.93 at pH 7.4 and 1.88 at pH 9.5. Notably, x approaches twice the value of 1, implying the presence of cryptic sulfur cycling—a phenomenon characterized by concurrent sulfate reduction and sulfide oxidation (Canfield et al., 2010; Hansel et al., 2015; Holmkvist et al., 2011).

As the anaerobic incubation progressed, the $Fe(II)_{tot}$ concentration decreased, possibly as a consequence of the Fe(II)-induced transformation of ferrihydrite (Jeon et al., 2003). This decrease in the $Fe(II)_{tot}$ concentration also explains the decreased sulfide concentration, based on the formation of crystalline iron sulfide minerals such as pyrite (Eq. (7)) (Hellige et al., 2012). Following successive aerobic and anaerobic incubations, the resulting Fe(III) minerals were again reduced during the second anaerobic period, exhibiting a same evolution of sulfide as shown in Fig. 3b. Interestingly, incubations with varying initial S° concentrations yielded similar results (Fig. S3). During the first anaerobic period, the S° concentration decreased rapidly together with the rapid formation of Fe(II) and sulfide. Moreover, a significant positive correlation was observed between the initial S° concentration and the Fe(II) peak concentration at 14 d, providing further evidence that S^0 played an important role in ferrihydrite reduction (Fig. S4).

Although pH has been shown to affect the sulfidation rate of iron (hydr)oxides, with the maximum rate at near neutral pH values (Peiffer et al., 1992; Poulton, 2003), the generation of Fe(II) from ferrihydrite reduction by biogenic sulfide occurred to the same extent at pH 7.4 and 9.5. This result can possibly be ascribed to the limitations associated with the sampling technique that was used, in that it was not possible to see small variations in the sulfidation rates of ferrihydrite at different pH values (Peiffer et al., 2015). In any case, the data confirm that biogenic sulfide from the transformation of S^0 promoted ferrihydrite reduction at both neutral and alkaline pH values.

3.2.3. *S^0-mediated ferrihydrite transformation*

XRD patterns demonstrated the mineralogical changes of ferrihydrite in the presence of S^0 (Fig. 7). During the first anaerobic incubation and

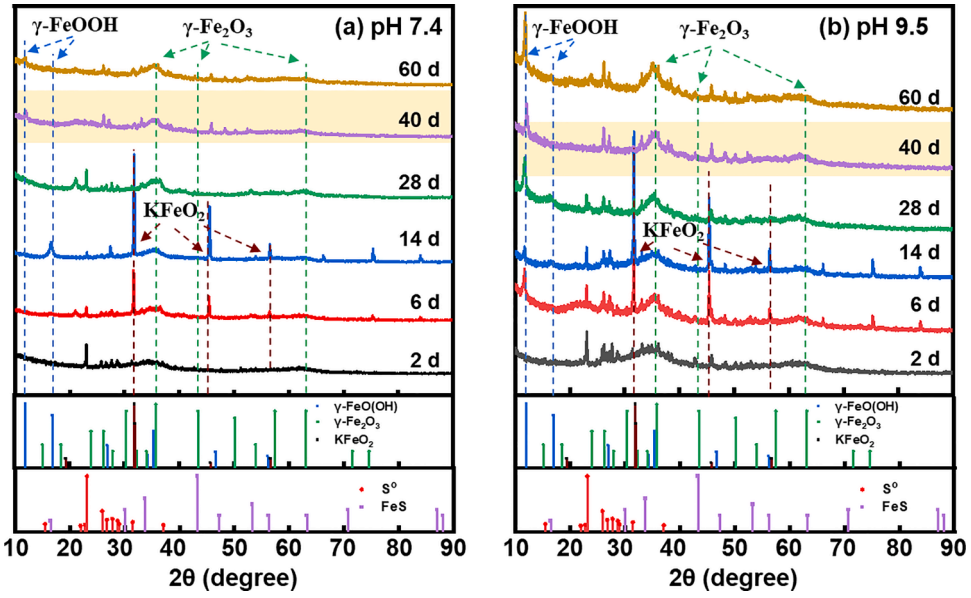

Fig. 7. XRD patterns of the solid phases with incubation proceeding at (a) pH 7.4 and (b) pH 9.5, respectively. The standard samples are referred to as PDF#75-1594 for FeO(OH), PDF#13-0458 for γ-Fe_2O_3, PDF#11-0151 for FeS, PDF#83-2153 for $KFeO_2$ and PDF#99-0066 for S^0). Noted that the samples at 40 d (shaded) were collected at the end of aerobic incubation, and the other samples were collected in anaerobic incubations.

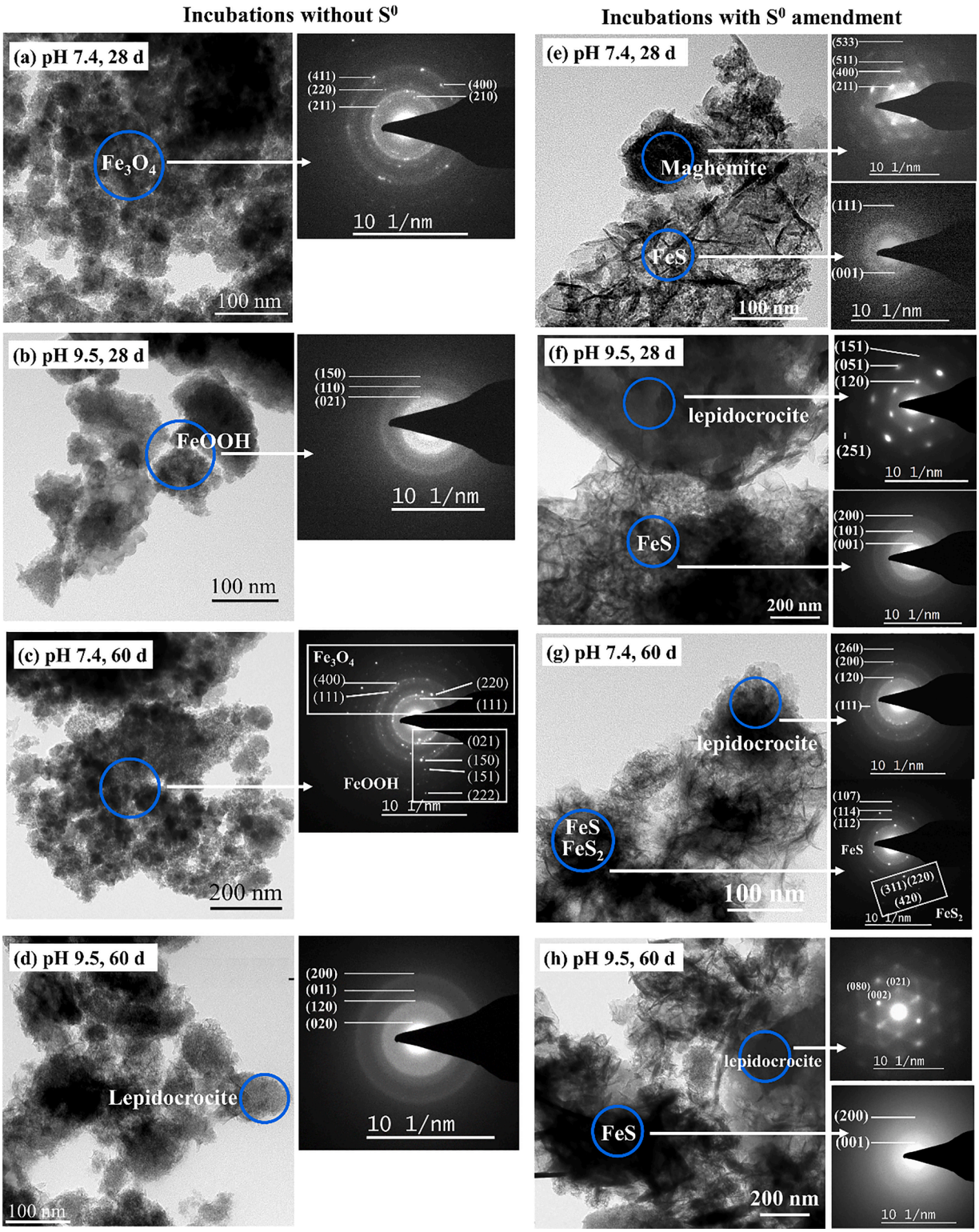

Fig. 8. HR-TEM images with electron diffraction patterns collected from incubations (a–d) without amendment of S^0 and (e–h) with amendment of S^0 at (a,b,e,f) 28 d and at (c,d,g,h) 60 d. Blue square indicates the region selected for selected area electron diffraction (SAED).

at pH 7.4, lepidocrocite formed at 14 d and subsequently transformed into maghemite (Fig. 7a). In contrast, at pH 9.5, lepidocrocite and maghemite were observed throughout the entire incubation period, regardless of whether anaerobic or aerobic conditions (Fig. 7b). The characteristic S^0 peak was found to rapidly decrease in intensity over time, confirming that S^0 was involved in the iron transformation process. At days 6 and 14 for both pH 7.4 and pH 9.5, two strong peaks appeared at 2θ=31.6 and 45.6, which may be attributed to an intermediate phase of $KFeO_2$. The formation of $KFeO_2$ was likely due to the incorporation of K ion from culture medium (0.028 g/L KCl and 0.030 g/L KH_2PO_4) into the lattice of iron (hydr)oxides during incubation process (Li and Shanks, 2009). HR-TEM images showed that, without S^0 addition, magnetite and lepidocrocite formed at both pH values under anaerobic conditions (Fig. 8a–d). Additionally, the HR-TEM images

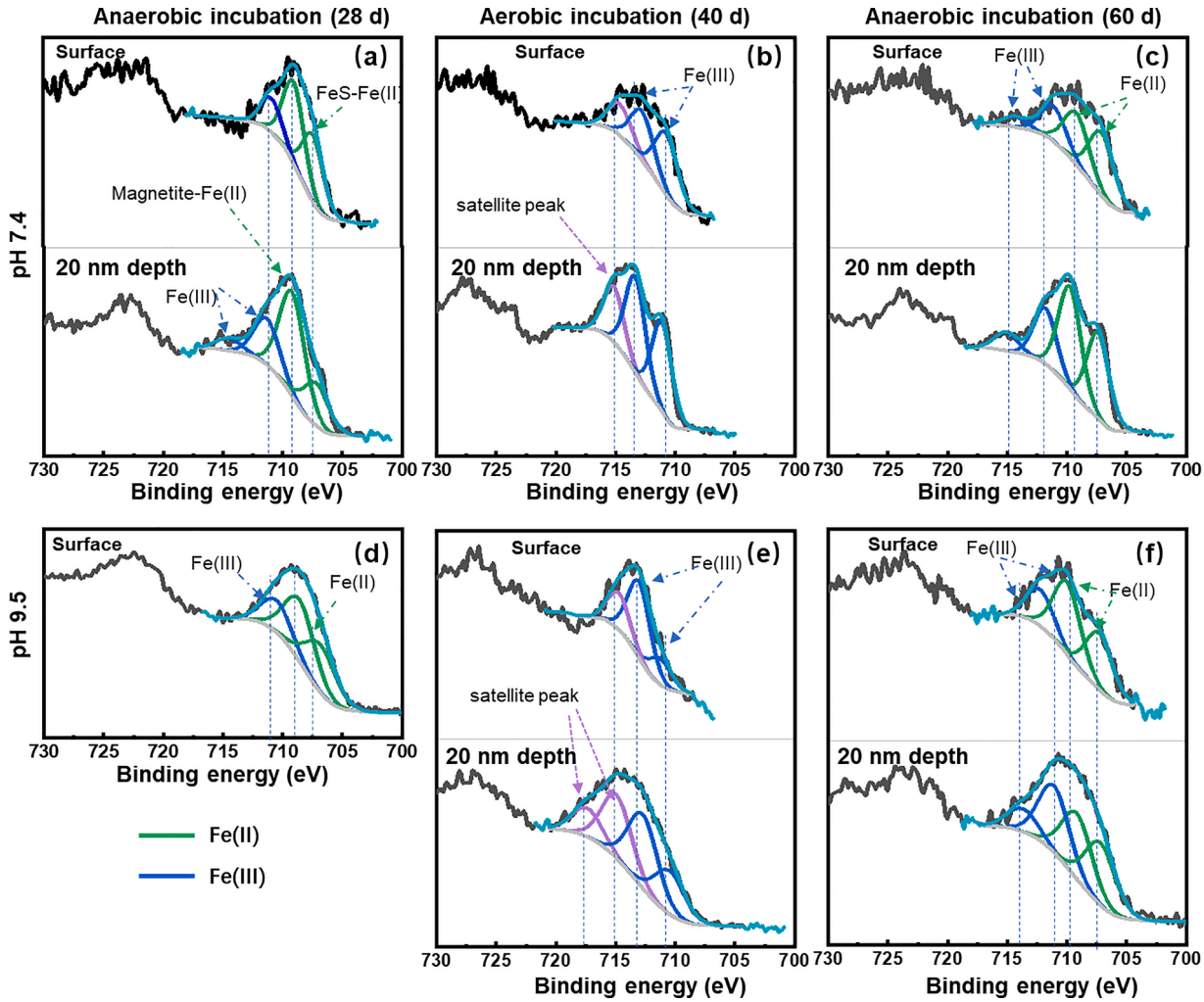

Fig. 9. Synchrotron XPS Fe 2p spectra of solid samples collected (a,d) at the end of first anaerobic incubation (28 d), (b,e) at the end of aerobic incubation (40 d) and (c,f) at the end of second anaerobic incubation (60 d). Spectra of (a,b,c) are samples collected at 7.4, and spectra of (d–f) are samples collected at 9.5. The probing depths were recorded at the surface and approximately 20 nm depth along the sample surface. The probing depths were recorded at the surface and 20 nm depth along the sample surface. Peak fitting for Fe 2p peaks was assigned based on literature-reported values summarized by Mullet et al. (2008), Tauson et al. (2008) and Wan et al. (2014).

indicated the formation of nanocrystalline FeS after 28 d of incubation with S^0 at pH 7.4 and 9.5. This material exhibited a fibrous morphology with the fibers having widths and lengths of approximately 1–3 nm and 50–100 nm, respectively (Fig. 8e and f). By the end of this whole incubation period (i.e., at 60 d), lepidocrocite and iron sulfide minerals were observed (Fig. 8g and h). The SAED pattern obtained from the FeS exhibited concentric rings and diffraction spots attributable to (111), (001), (200), and (101) diffraction planes (Fig. 8e, f and h) (Malek et al., 2018). The SAED pattern also established the cubic structure of the maghemite phase (Fig. 8e) and the diffraction planes that were observed (e.g., the (200), (011), (020) and (120) planes) were similar to those of a lepidocrocite-rich structure (Fig. 8f–h) (Iconaru et al., 2012).

The synchrotron-based XPS analysis also revealed changes in the redox states of the surface Fe of the various minerals during the incubation. At the end of the two anaerobic incubations (28 and 60 d), peaks appeared at 711–714 and 709.3 eV that were attributed to Fe(III) in lepidocrocite and Fe(II) in magnetite, respectively (Grosvenor et al., 2004b; Wan et al., 2014) (Fig. 9a, c, d and f). An additional peak at 707.6 eV was ascribed to surface Fe(II)-FeS (Tauson et al., 2008; Wan et al., 2014) and was obtained regardless of the pH (Fig. 9a, c, d and f). After 12 d of aerobic incubation, characteristic Fe(III) peaks (711–714 eV) and satellite peaks (approximately 715 and 717 eV) (Grosvenor et al., 2004a; Mullet et al., 2008) appeared in the spectra (Fig. 9b and e).

These results collectively suggest that the biotransformation of S^0 drove the transformation of ferrihydrite under the fluctuating redox conditions. Specifically, biogenic sulfide reduced ferrihydrite to generate iron sulfide precipitates under anaerobic conditions and various crystalline iron (hydr)oxides (i.e., lepidocrocite and maghemite) under both anaerobic and aerobic conditions. The exchange of redox conditions between the anaerobic and aerobic conditions would be expected to interrupt the ripening process of iron (hydr)oxides towards mineral with higher crystallinity and stability and thus promote the reduction of these iron (hydr)oxides (Peiffer et al., 2021; Winkler et al., 2018; Zhao et al., 2023). However, the unambiguous determination of the composition and structure of each of the various iron (hydr)oxide mineral products will require the use of advanced techniques such as X-ray absorption spectroscopy, Mössbauer spectroscopy, and cryo-electron microscopy in future studies.

After redox fluctuations, a fraction of the initial ferrihydrite transformed to more crystalline iron (hydr)oxides (e.g., lepidocrocite, maghemite) and iron sulfides. These secondary iron minerals, compared to ferrihydrite, which is one of the most reactive iron minerals, are likely to retard the redox reactions of iron with environmentally relevant components (Cornell and Schwertmann, 2003). On the other hand, during the oxic period, the phosphate present in the culture medium (0.22 mM) may coprecipitate with Fe(II) generated from the anoxic

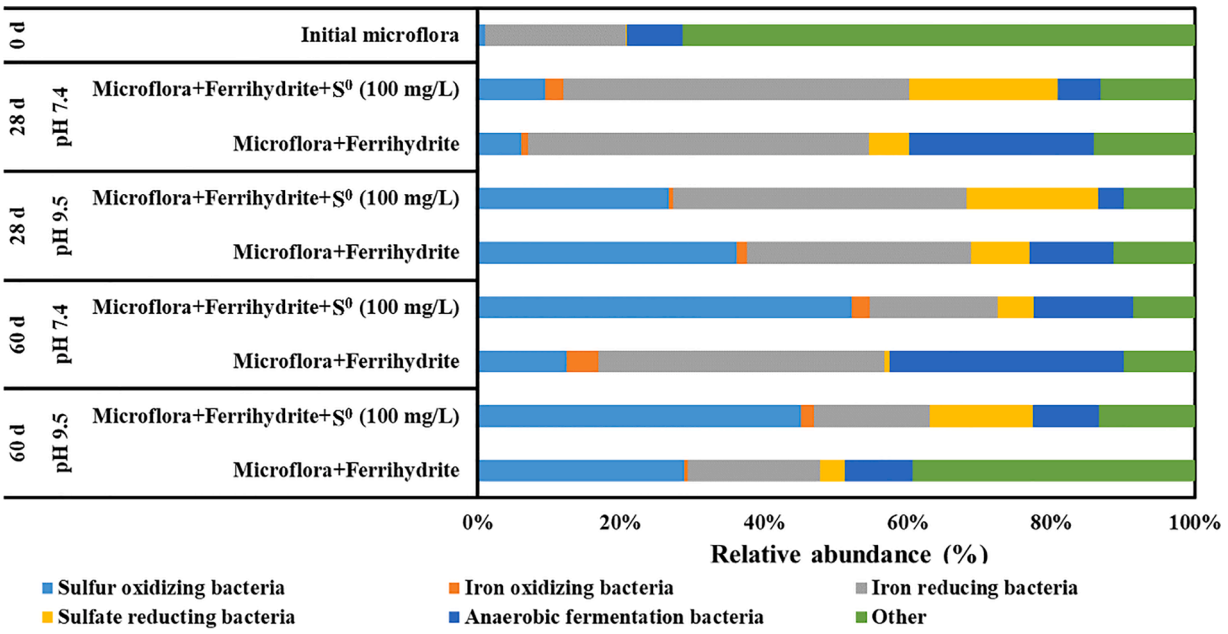

Fig. 10. Evolution of the bacterial community under different incubation conditions. The bacterial community classified by the functionality was calculated based on high-throughput sequencing of the 16S rDNA gene, and clustered with 97 % similarity by Usearch software. Details of bacterial community can be found in Figs. S6–S11.

period. The phosphate coprecipitated ferric (hydr)oxides generally increase the reactivity and dissolution rate of ferric (hydr)oxides towards sulfide (Kraal et al., 2022; Kraal et al., 2019). While phosphate coprecipitated ferric (hydr)oxides were not detected in XRD and HR-TEM, we cannot completely rule out its presence as well as its potential influence on the subsequent interaction of iron (hydr)oxides with sulfide. The abovementioned transformations of ferrihydrite collectively raise the question of whether, after several redox fluctuations, the redox reactions between iron (hydr)oxides and sulfide can still occur to a high extent. To this end, we compared the reactivity between iron (hydr)oxides and sulfide before and after the oxic period. The generation rate of Fe(II) was used as a good proxy for the reaction rate between sulfide and iron (hydr)oxides (Peiffer et al., 1992; Poulton et al., 2004). The generation rates of Fe(II) were obtained though fitting selected data points under the first and second anaerobic conditions following Amstaetter et al. (2012) (Fig. S5). The results revealed that the Fe(II) generation rates in the first anaerobic incubation were 0.395 mM/d and 0.475 mM/d at pH 7.4 and 9.5, respectively. While in the second anaerobic incubation, Fe (II) generation rates were 0.306 mM/d and 0.368 mM/d at pH 7.4 and 9.5, respectively, which were approximately 25 % lower than those in the first anaerobic incubation. Interestingly, the generation rates of Fe (II) at pH 7.4 are lower than those at pH 9.5, contracting with previous report that sulfidation rate of Fe(III) reaches its highest rate at neutral pH (Peiffer et al., 1992; Poulton et al., 2004). This difference is likely due to the higher generation rate of sulfide from S^0 reduction at higher pH values (Flynn et al., 2014). Taken together, our results suggest that under fluctuating redox conditions, the degree of interactions between iron (hydr)oxides and sulfide decreased by less than 25 % compared to the interactions in the first anaerobic incubation period, but still remained a sustainable electron transfer process through coupled iron and sulfur cycling, which could govern the redox transformation of contaminants in natural and engineered systems.

3.3. Microbial community dynamics

To explore the role of bacteria in the transformation of sulfur and iron (hydr)oxides under different conditions, we used the 16S rDNA based technique to monitor the structure of the bacterial community throughout the experimental trials (Figs. 10 and S6–S11). The results showed that iron-reducing bacteria accounted for a principal proportion (16.2–48.3 %) of the bacterial community throughout the whole incubation period (Fig. 10). Despite the high abundance of iron-reducing bacteria, the wet chemical result suggested that the bio-reduction of ferrihydrite occurred at a negligible extent and is favored at neutral pH (Fig. 6a), consistent with previous report by Flynn et al. (2014). The incorporation of S^0 promoted the proliferation of both sulfur-oxidizing and sulfur-reducing bacteria. After 28 d of incubation at pH 7.4, the proportions of sulfur-oxidizing and sulfur-reducing bacteria increased from negligible levels (< 0.1 %) to 9.4 % and 20.7 %, respectively (Fig. 10), demonstrating the promotion of sulfur-based metabolic pathways in the system.

In the incubations with S^0, the abundance of sulfur-metabolism bacteria exceeds that of iron-metabolism bacteria. The total proportion of sulfur-metabolism bacteria increased from 30.1 % at 28 d to 55.2 % at 60 d In contrast, the total proportion of iron- metabolism bacteria decreased from 50.8 % at 28 d to 20.4 % at 60 d at pH 7.4 (Fig. 10). Thus, we proposed that sulfur cycling may precede iron cycling under the fluctuating redox conditions. This abundance of sulfur-oxidizing bacteria might be responsible for the formation of sulfate, since chemical oxidation of sulfide by iron (hydr)oxides is unlikely to produce sulfate (Poulton, 2003; Wan et al., 2014). Furthermore, following a 60 d aerobic-anaerobic cycle at pH 9.5, the proportion of sulfur-reducing bacteria in the presence of S^0 (14.3 %) was significantly higher than that obtained without S^0 (3.4 %) (Fig. 10). This increase in the number of sulfur-reducing bacteria explains the enhanced production of Fe(II) compared with that observed in the incubations without S^0. Under anaerobic conditions, regardless of the addition of S^0, the proportions of iron-reducing bacteria were at the same level as each other, which does not explain the higher extent of Fe(II) production in incubations with added S^0. These data suggest that biogenic sulfide promoted Fe(III) reduction in the incubations that incorporated S^0. Overall, microbial-mediated elemental sulfur disproportionation contributed to the cycling of sulfur and iron under fluctuating redox conditions.

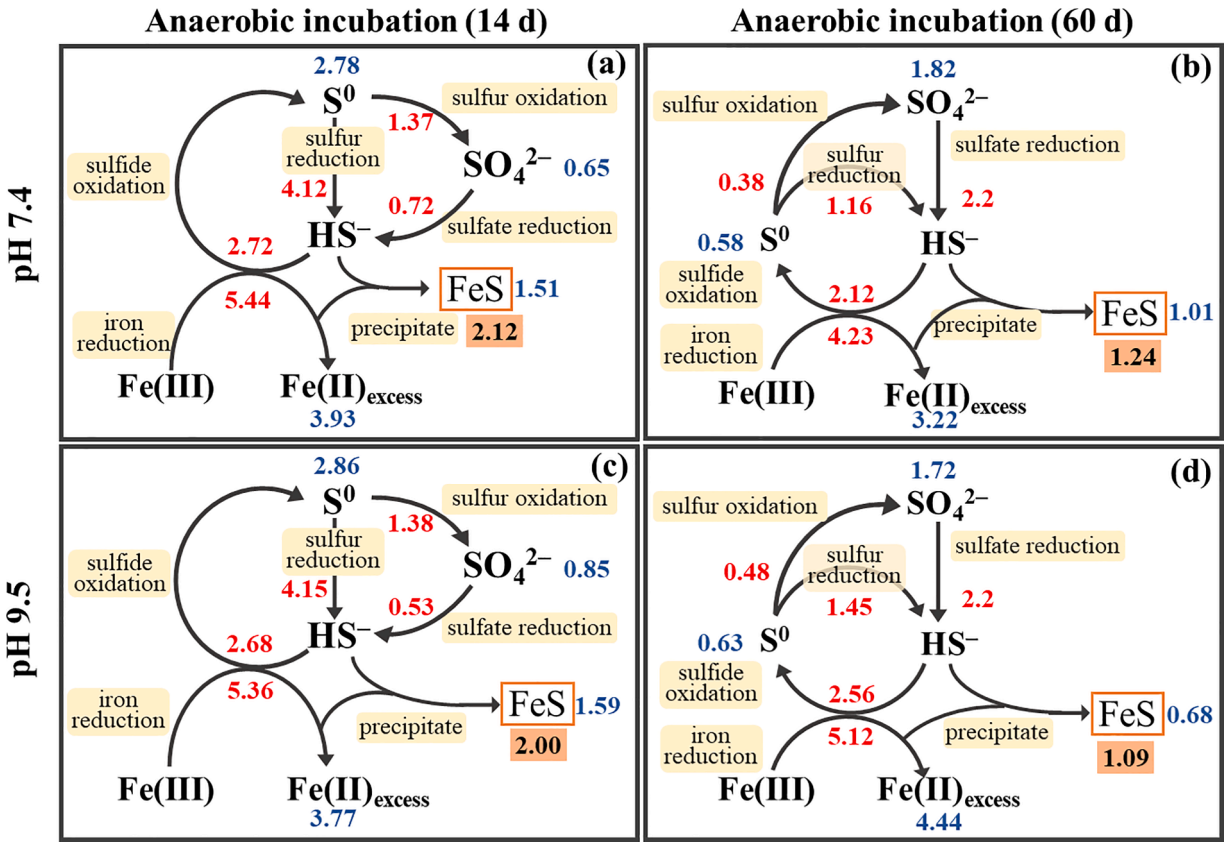

Fig. 11. Conceptual model of proposed reaction network that sustain redox reactions between iron and sulfur species at pH 7.4 and 9.5 under anaerobic conditions (a and c at 14 d, b and d at 60 d). The text in yellow shadow indicates the reaction pathway. Values shown in dark-blue are the concentrations (in mM) measured at the selected reaction points. Values shown in red at arrows are the amounts of transformed pathway calculated *via* chemical stoichiometries (see details in Table S2). The value in orange shadow is the calculated S(-II) concentration. $Fe(II)_{tot}$ is measured as extractable in 1 M HCl extraction, including sulfide associated Fe(II) and excess Fe(II) that associated with iron (hydr)oxides. Residual sulfide is measured as acid volatile sulfide (since free sulfide is not detected, the measured sulfide also points to the concentration of FeS). Sulfide that reacted with Fe(III) to produce S° calculated *via* $Fe(II)_{tot}$ concentration; sulfide formation is calculated *via* S^0 disproportionation and sulfate reduction. S^0 regeneration is calculated stoichiometrically *via* Eq. (S1) based on $Fe(II)_{tot}$ concentration. Sulfate formation is calculated as S^0 disproportionation, sulfate consumption through sulfate reduction is calculated *via* the difference between sulfate formation and residual sulfate concentration. To simplify the calculation, bioreduction of Fe(III) is not taken into account due to its minor contribution to Fe(II) generation.

3.4. Mechanisms of microbial-mediated S^0 transformation

Based on the data obtained in this work, a mechanism for S^0 metabolism under fluctuating redox conditions can be proposed. Under anaerobic conditions, the microbial disproportionation of S^0 in the presence of iron (hydr)oxides produces sulfide and sulfate, with sulfate becoming further reduced by sulfate-reducing bacteria to sulfide. The biogenic sulfide drives the reduction of iron (hydr)oxides (Eq. (5)), and iron (hydr)oxides, in turn, promoted further disproportionation of S^0 by scavenging sulfide. After an oxic period, upon being subjected to renewed anaerobic conditions, the sulfate-reducing bacteria reduce sulfate to sulfide to continually drive the cycling of sulfur, as well as the coupled transformation of iron (hydr)oxides.

To quantitatively substantiate this proposed mechanism, mass balance calculations were performed *via* redox reactions. To do this we took the results at 14 d (the first anaerobic conditions) and 60 d (the second anaerobic conditions) for analysis. The data at 14 d was selected because all reactants reached their peak concentration, indicating the highest reaction extent. After 14 d, the concentrations of sulfide, total Fe(II), and sulfate began to decline, suggesting a transformation of these substances, making our calculation more complicated. Accordingly, the data at 60 d was selected because it represented the end situation of the system. The data in the aerobic condition was not chosen, because the involution of O_2 challenged our calculation. Due to the cryptic sulfur cycling in which biogenic sulfide from S^0 disproportionation can be reoxidized by Fe(III) to replenish the S^0 pool (Canfield et al., 2010; Hansel et al., 2015; Holmkvist et al., 2011), it becomes a significant challenge to determine the number of replenishment cycles for S^0. Consequently, it appears unfeasible to accurately quantify the electron transfer process through S^0 consumption. An alternative and reasonable approach for quantifying electron transfer processes would entail the examination of Fe(II) generation. While we cannot quantitatively determine the extent of Fe(III) bioreduction, we estimate that it is a minor contributor compared to abiotic reduction of Fe(III) by sulfide (Fig. 6) (Flynn et al., 2014; Hansel et al., 2015). Consequently, to simplify the calculation of redox reactions between Fe and S species, the bioreduction of Fe(III) was not taken into account due to its minor contribution. Thus, we determined the amounts of sulfide that reacted with Fe(III) based on the amount of generated Fe(II). By employing this approach (see Text S7 for details), we estimated the FeS accumulation using measured data of relevant species (Fig. 11). The estimated sulfide accumulation (denoted as FeS in Fig. 11) is slightly higher than the measured sulfide concentration (Table S2). The obtained S recovery and percent discrepancy of S(-II) ranged from 80.4 % to 100.3 % and 7.4 % to 19.6 %, respectively, suggesting a reasonable balance. Nevertheless, there are some uncertainties in our calculation, including undetected sulfur species (i.e., thiosulfate), incompletely recovered species (i.e., the Fe(II) and S(-II) that contained in crystalline iron sulfide minerals), as well as some uncharacterized carbon or bacteria involved reactions. To achieve a more accurate mass balance calculation, a more detailed and

comprehensive reaction mechanism is required in future. Taken together, this proposed mechanism suggests that under fluctuating redox conditions, sulfur-based transformation maintained a sustainable electron transfer process in the coupled cycling of sulfur and iron, potentially governing a span of iron-sulfur relevant pollutants transformation under fluctuating redox conditions.

3.5. Environmental significance

Our experiments illustrate that after redox fluctuations, reactions between iron (hydr)oxides and sulfide can remain a sustainable electron transfer process driven by sulfur metabolism, in which S^0 acts as a novel electron pump to promote these reactions, especially at alkaline pH values that may greatly inhibit iron cycling (Bronner et al., 2023; Flynn et al., 2014). Under anaerobic conditions, the biotransformation of S^0 produces sulfide and sulfate. The sulfide subsequently reductively dissolve iron (hydr)oxides and thus affects the transformation of certain pollutants (Borch et al., 2010; Zhang et al., 2022). Importantly, redox fluctuations can impede the transformation of ferrihydrite to highly crystalline iron (hydr)oxides (Peiffer et al., 2021). This characteristic allows for sustained iron-based redox reactions, including the coupled cycling of sulfur, in response to environmental changes. Moreover, in the presence of iron (hydr)oxides, sulfate generation under anaerobic conditions enables the anaerobic oxidation of methane to carbon dioxide (Kappler et al., 2021; Milucka et al., 2012), thus potentially affecting global warming. Overall, the present study demonstrates the critical role of S^0 in sulfur and iron cycling under fluctuating redox conditions, suggesting new approaches to bio-remediation. For example, in specific environments with low natural organic matter but abundant sulfur and iron, such as aquifers where the activity of bacteria may be restricted, the acetate or sulfur-reducing bacteria can be introduced to stimulate the cycling of sulfur and iron and effectively mediate the transformation of pollutants. As organic carbon is inevitably involved in the transformation of iron and sulfur, the mass balance analysis in the present study might be not fully comprehensive. Consequently, further research is needed to identify the specific contribution of organic matter to the redox interactions between iron and sulfur, which would facilitate advancements in the biotransformation of relevant pollutants.

4. Conclusions

This study reveals that in the copresence of ferrihydrite and S^0, the biotransformation of S^0 is the dominant electron-shuttling process and play a major role in the reduction of ferrihydrite under fluctuating redox conditions. Ferrihydrite, in turn, promotes the disproportionation S^0 by scavenging biogenic sulfide through reoxidation of sulfide to S^0 and precipitating sulfide as iron sulfide minerals, thus maintaining the cycling of sulfur. The cryptic sulfur cycling enhanced Fe(III) reduction. Further, the results also demonstrate that the active redox reactions between sulfur and iron species are sustainable after a sequential anaerobic-aerobic-anaerobic incubation as in the first anaerobic condition. This study provides valuable knowledge by highlighting that redox fluctuations can maintain a sustainable electron transfer process between bio-mediated sulfur and iron cycling.

Declaration of Competing Interest

We (all authors) declare that we have no known competing financial interests or personal relationships that could have appeared to influence the work reported in this paper.

Data availability

Data will be made available on request.

Acknowledgments

This study was supported by the National Natural Science Foundation of China (No. 42177237). XPS analyses were performed at the Catalysis and Surface Science Endstation at the BL11U beamline in the National Synchrotron Radiation Laboratory (NSRL) in Hefei, China.

Supplementary materials

Supplementary material associated with this article can be found, in the online version, at doi:10.1016/j.watres.2023.120589.

References

Amstaetter, K., Borch, T., Kappler, A., 2012. Influence of humic acid imposed changes of ferrihydrite aggregation on microbial Fe(III) reduction. Geochim. Cosmochim. Acta 85, 326–341.
Bai, Y., Wang, S., Zhussupbekova, A., Shvets, I.V., Lee, P.-H., Zhan, X., 2023. High-rate iron sulfide and sulfur-coupled autotrophic denitrification system: nutrients removal performance and microbial characterization. Water Res. 231, 119619.
Baraket, L., Ghorbel, A., Grange, P., 2007. Selective catalytic reduction of NO by ammonia on V_2O_5–SO_4^{2-}/TiO_2 catalysts prepared by the sol–gel method. Appl. Catal. B 72 (1), 37–43.
Bingjie, O., Xiancai, L., Huan, L., Juan, L., Tingting, Z., Xiangyu, Z., Jianjun, L., Rucheng, W., 2014. Reduction of jarosite by *Shewanella oneidensis* MR-1 and secondary mineralization. Geochim. Cosmochim. Acta 124, 54–71.
Borch, T., Kretzschmar, R., Kappler, A., Cappellen, P.V., Ginder-Vogel, M., Voegelin, A., Campbell, K., 2010. Biogeochemical redox processes and their impact on contaminant dynamics. Environ. Sci. Technol. 44 (1), 15–23.
Bronner, R., Thompson, K., Dreher, C., Runge, E., Voggenreiter, E., Shuster, J., Wan, B., Joshi, P., Fischer, S., Duda, J.P., Kappler, A., Mansor, M., 2023. Co-reduction of Fe (III) and S^0 drives Fe-S biomineral formation and phosphate mobilisation. Geochem. Perspect. Lett. 24, 27–32.
Burton, E.D., Bush, R.T., Sullivan, L.A., 2006. Elemental sulfur in drain sediments associated with acid sulfate soils. Appl. Geochem. 21 (7), 1240–1247.
Canfield, D.E., Stewart, F.J., Thamdrup, B., De Brabandere, L., Dalsgaard, T., Delong, E. F., Revsbech, N.P., Ulloa, O., 2010. A cryptic sulfur cycle in oxygen-minimum–zone waters off the Chilean coast. Science 330 (6009), 1375–1378.
Cline, J.D., 1969. Spectrophotometric determination of hydrogen sulfide in natural waters. Limnol. Oceanogr. 14, 454–458.
Cornell, R., Schwertmann, U., 2003. The Iron Oxides: Structure, Properties, Reactions, Occurrences, and Uses. Wiley-vch (Vol. 664)Weinheim.
Dahl, C., Friedrich, C.G., 2008. Microbial Sulfur Metabolism. Springer.
Ding, H., Li, B., Zareen, S., Li, G., Tu, Y., Zhang, D., Cao, X., Xu, Q., Yang, S., Tait, S.L., Zhu, J., 2020. *In situ* investigations of Al/Perovskite interfacial structures. ACS Appl. Mater. Interfaces 12 (25), 28861–28868.
El Houari, A., Ranchou-Peyruse, M., Ranchou-Peyruse, A., Dakdaki, A., Guignard, M., Idouhammou, L., Bennisse, R., Bouterfass, R., Guyoneaud, R., Qatibi, A.-I., 2017. *Desulfobulbus oligotrophicus* sp. nov., a sulfate-reducing and propionate-oxidizing bacterium isolated from a municipal anaerobic sewage sludge digester. Int. J. Syst. Evol. Micr. 67 (2), 275–281.
Finster, K., 2008. Microbiological disproportionation of inorganic sulfur compounds. J. Sulfur Chem. 29 (3–4), 281–292.
Flynn, T.M., O'Loughlin, E.J., Mishra, B., DiChristina, T.J., Kemner, K.M., 2014. Sulfur-mediated electron shuttling during bacterial iron reduction. Science 344 (6187), 1039–1042.
Ginn, B., Meile, C., Wilmoth, J., Tang, Y., Thompson, A., 2017. Rapid iron reduction rates are stimulated by high-amplitude redox fluctuations in a tropical forest soil. Environ. Sci. Technol. 51 (6), 3250–3259.
Grosvenor, A., Kobe, B., Biesinger, M.C., McIntyre, N., 2004a. Investigation of multiplet splitting of Fe2p XPS spectra and bonding in iron compounds. Surf. Interface Anal. 36 (12), 1564–1574.
Grosvenor, A., Kobe, B., McIntyre, N., 2004b. Examination of the oxidation of iron by oxygen using X-ray photoelectron spectroscopy and QUASESTM. Surf. Sci. 565 (2–3), 151–162.
Hampton, M.A., Plackowski, C., Nguyen, A.V., 2011. Physical and chemical analysis of elemental sulfur formation during galena surface oxidation. Langmuir 27 (7), 4190–4201.
Hansel, C.M., Lentini, C.J., Tang, Y., Johnston, D.T., Wankel, S.D., Jardine, P.M., 2015. Dominance of sulfur-fueled iron oxide reduction in low-sulfate freshwater sediments. ISME J. 9 (11), 2400–2412.
Hao, O.J., Chen, J.M., Huang, L., Buglass, R.L., 1996. Sulfate-reducing bacteria. Crit. Rev. Environ. Sci. Technol. 26 (2), 155–187.
He, J., Zhang, B., Wang, Y.N., Chen, S., Dong, H., 2023. Vanadate bio-detoxification driven by pyrrhotite with secondary mineral formation. Environ. Sci. Technol 57 (4), 1807–1818.
Hellige, K., Pollok, K., Larese-Casanova, P., Behrends, T., Peiffer, S., 2012. Pathways of ferrous iron mineral formation upon sulfidation of lepidocrocite surfaces. Geochim. Cosmochim. Acta 81, 69–81.
Holmkvist, L., Ferdelman, T.G., Jørgensen, B.B., 2011. A cryptic sulfur cycle driven by iron in the methane zone of marine sediment (Aarhus Bay, Denmark). Geochim. Cosmochim. Acta 75 (12), 3581–3599.

Iconaru, S.L., Prodan, A.M., Motelica-Heino, M., Sizaret, S., Predoi, D., 2012. Synthesis and characterization of polysaccharide-maghemite composite nanoparticles and their antibacterial properties. Nanoscale Res. Lett. 7 (1), 576.
Jeon, B.-H., Dempsey, B.A., Burgos, W.D., 2003. Kinetics and mechanisms for reactions of Fe(II) with iron(III) oxides. Environ. Sci. Technol. 37 (15), 3309–3315.
Jørgensen, B.B., 1990a. The sulfur cycle of freshwater sediments: role of thiosulfate. Limnol. Oceanogr. 35 (6), 1329–1342.
Jørgensen, B.B., 1990b. A thiosulfate shunt in the sulfur cycle of marine sediments. Science 249 (4965), 152–154.
Jørgensen, B.B., Findlay, A.J., Pellerin, A., 2019. The biogeochemical sulfur cycle of marine sediments. Front. Microbiol. 10, 1–27.
Kappler, A., Bryce, C., Mansor, M., Lueder, U., Byrne, J.M., Swanner, E.D., 2021. An evolving view on biogeochemical cycling of iron. Nat. Rev. Microbiol. 19 (6), 360–374.
Karimian, N., Johnston, S.G., Burton, E.D., 2018. Iron and sulfur cycling in acid sulfate soil wetlands under dynamic redox conditions: a review. Chemosphere 197, 803–816.
Kleinjan, W.E., de Keizer, A., Janssen, A.J.H., 2005. Equilibrium of the reaction between dissolved sodium sulfide and biologically produced sulfur. Colloids Surf. B 43 (3), 228–237.
Kojima, H., Watanabe, T., Fukui, M., 2016. *Sulfuricaulis limicola gen.* nov., sp. nov., a sulfur oxidizer isolated from a lake. Int. J. Syst. Evol. Micr. 66 (1), 266–270.
Kraal, P., van Genuchten, C.M., Behrends, T., 2022. Phosphate coprecipitation affects reactivity of iron (oxyhydr)oxides towards dissolved iron and sulfide. Geochim. Cosmochim. Acta 321, 311–328.
Kraal, P., van Genuchten, C.M., Behrends, T., Rose, A.L., 2019. Sorption of phosphate and silicate alters dissolution kinetics of poorly crystalline iron (oxyhydr)oxide. Chemosphere 234, 690–701.
Li, B., Zhang, S., Liao, P., Liu, P., Ye, Z., Liu, C., 2022. NOM-induced dissolution of $Cr_xFe_{1-x}(OH)_3$ precipitates and formation of Cr(III)-NOM-Fe colloids under oxic and anoxic conditions. ACS Earth Space Chem. 6 (12), 2995–3006.
Li, Z., Shanks, B.H., 2009. Stability and phase transitions of potassium-promoted iron oxide in various gas phase environments. Appl. Catal. A Gen. 354 (1–2), 50–56.
Liao, P., Li, W., Jiang, Y., Wu, J., Yuan, S., Fortner, J.D., Giammar, D.E., 2017. Formation, aggregation, and deposition dynamics of NOM-iron colloids at anoxic–oxic interfaces. Environ. Sci. Technol. 51 (21), 12235–12245.
Malek, T.J., Chaki, S.H., Deshpande, M., 2018. Structural, morphological, optical, thermal and magnetic study of mackinawite FeS nanoparticles synthesized by wet chemical reduction technique. Phys. B Condens. Matter 546, 59–66.
Milucka, J., Ferdelman, T.G., Polerecky, L., Franzke, D., Wegener, G., Schmid, M., Lieberwirth, I., Wagner, M., Widdel, F., Kuypers, M.M.M., 2012. Zero-valent sulphur is a key intermediate in marine methane oxidation. Nature 491 (7425), 541–546.
Mullet, M., Khare, V., Ruby, C., 2008. XPS study of Fe(II)-Fe(III) (oxy)hydroxycarbonate green rust compounds. Surf. Interface Anal. 40 (3–4), 323–328.
Nandasiri, M.I., Camacho-Forero, L.E., Schwarz, A.M., Shutthanandan, V., Thevuthasan, S., Balbuena, P.B., Mueller, K.T., Murugesan, V., 2017. *In situ* chemical imaging of solid-electrolyte interphase layer evolution in Li–S batteries. Chem. Mater. 29 (11), 4728–4737.
O'Day, P.A., Vlassopoulos, D., Root, R., Rivera, N., 2004. The influence of sulfur and iron on dissolved arsenic concentrations in the shallow subsurface under changing redox conditions. Proc. Natl. Acad. Sci. 101 (38), 13703–13708.
Peiffer, S., Behrends, T., Hellige, K., Larese-Casanova, P., Wan, M., Pollok, K., 2015. Pyrite formation and mineral transformation pathways upon sulfidation of ferric hydroxides depend on mineral type and sulfide concentration. Chem. Geol. 400, 44–55.
Peiffer, S., Dos Santos Afonso, M., Wehrli, B., Gaechter, R., 1992. Kinetics and mechanism of the reaction of hydrogen sulfide with lepidocrocite. Environ. Sci. Technol. 26 (12), 2408–2413.
Peiffer, S., Kappler, A., Haderlein, S.B., Schmidt, C., Byrne, J.M., Kleindienst, S., Vogt, C., Richnow, H.H., Obst, M., Angenent, L.T., Bryce, C., McCammon, C., Planer-Friedrich, B., 2021. A biogeochemical–hydrological framework for the role of redox-active compounds in aquatic systems. Nat. Geosci. 14 (5), 264–272.
Philippot, P., Van Zuilen, M., Lepot, K., Thomazo, C., Farquhar, J., Van Kranendonk, M. J., 2007. Early Archaean microorganisms preferred elemental sulfur, not sulfate. Science 317 (5844), 1534–1537.
Poser, A., Lohmayer, R., Vogt, C., Knoeller, K., Planer-Friedrich, B., Sorokin, D., Richnow, H.-H., Finster, K., 2013. Disproportionation of elemental sulfur by haloalkaliphilic bacteria from soda lakes. Extremophiles 17 (6), 1003–1012.
Poulton, S.W., 2003. Sulfide oxidation and iron dissolution kinetics during the reaction of dissolved sulfide with ferrihydrite. Chem. Geol. 202 (1), 79–94.
Poulton, S.W., Krom, M.D., Raiswell, R., 2004. A revised scheme for the reactivity of iron (oxyhydr)oxide minerals towards dissolved sulfide. Geochim. Cosmochim. Acta 68 (18), 3703–3715.
Qiu, Y.Y., Zhang, L., Mu, X., Li, G., Guan, X., Hong, J., Jiang, F., 2020. Overlooked pathways of denitrification in a sulfur-based denitrification system with organic supplementation. Water Res. 169, 115084.
Schwertmann, U., Cornell, R.M., 2008. Iron Oxides in the Laboratory: Preparation and Characterization. John Wiley & Sons.
Sharma, N., Wang, Z., Catalano, J.G., Giammar, D.E., 2022. Dynamic responses of trace metal bioaccessibility to fluctuating redox conditions in wetland soils and stream sediments. ACS Earth Space Chem. 6 (5), 1331–1344.
Shi, C., Cui, Y., Lu, J., Zhang, B., 2020. Sulfur-based autotrophic biosystem for efficient vanadium(V) and chromium(VI) reductions in groundwater. Chem. Eng. J. 395, 124972.
Shimoshige, H., Kobayashi, H., Shimamura, S., Miyazaki, M., Maekawa, T., 2022. Fundidesulfovibrio magnetotacticus sp. nov., a sulphate-reducing magnetotactic bacterium, isolated from sediments and freshwater of a pond. Int. J. Syst. Evol. Microbiol. 72 (9), 1–11.
Tamura, H., Goto, K., Yotsuyanagi, T., Nagayama, M., 1974. Spectrophotometric determination of iron(II) with 1,10-phenanthroline in the presence of large amounts of iron(III). Talanta 21 (4), 314–318.
Tauson, V.L., Babkin, D.N., Lustenberg, E.E., Lipko, S.V., Parkhomenko, I.Y., 2008. Surface typochemistry of hydrothermal pyrite: electron spectroscopic and scanning probe microscopic data. I. Synthetic pyrite. Geochem. Int. 46 (6), 565–577.
Thamdrup, B., Finster, K., Hansen, J.W., Bak, F., 1993. Bacterial disproportionation of elemental sulfur coupled to chemical reduction of iron or manganese. Appl. Environ. Microbiol. 59 (1), 101–108.
Thompson, A., Chadwick, O.A., Rancourt, D.G., Chorover, J., 2006. Iron-oxide crystallinity increases during soil redox oscillations. Geochim. Cosmochim. Acta 70 (7), 1710–1727.
Troelsen, H., Jørgensen, B.B., 1982. Seasonal dynamics of elemental sulfur in two coastal sediments. Estuar. Coast. Shelf Sci. 15 (3), 255–266. Estuar. Coast. Shelf S.
Wan, M., Shchukarev, A., Lohmayer, R., Planer-Friedrich, B., Peiffer, S., 2014. Occurrence of surface polysulfides during the interaction between ferric (hydr) oxides and aqueous sulfide. Environ. Sci. Technol. 48 (9), 5076–5084.
Wang, J., Dai, J., Chen, G., Jiang, F., 2022. Role of sulfur biogeochemical cycle in mercury methylation in estuarine sediments: a review. J. Hazard. Mater. 423, 126964.
Wang, Q., Wang, J., Wang, X., Kumar, N., Pan, Z., Peiffer, S., Wang, Z., 2023a. Transformations of ferrihydrite–extracellular polymeric substance coprecipitates driven by dissolved sulfide: interrelated effects of carbon and sulfur loadings. Environ. Sci. Technol. 57 (10), 4342–4353.
Wang, S., Lu, Q., Liang, Z., Yu, X., Lin, M., Mai, B., Qiu, R., Shu, W., He, Z., Wall, J.D., 2023b. Generation of zero-valent sulfur from dissimilatory sulfate reduction in sulfate-reducing microorganisms. Proc. Natl. Acad. Sci. 120 (20), e2220725120.
Winkler, P., Kaiser, K., Thompson, A., Kalbitz, K., Fiedler, S., Jahn, R., 2018. Contrasting evolution of iron phase composition in soils exposed to redox fluctuations. Geochim. Cosmochim. Acta 235, 89–102.
Yu, Z.-G., Peiffer, S., Göttlicher, J., Knorr, K.-H., 2015. Electron transfer budgets and kinetics of abiotic oxidation and incorporation of aqueous sulfide by dissolved organic matter. Environ. Sci. Technol. 49 (9), 5441–5449.
Yücel, M., Konovalov, S.K., Moore, T.S., Janzen, C.P., Luther, G.W., 2010. Sulfur speciation in the upper Black Sea sediments. Chem. Geol. 269 (3), 364–375.
Zhang, S., Peiffer, S., Liao, X., Yang, Z., Ma, X., He, D., 2022. Sulfidation of ferric (hydr) oxides and its implication on contaminants transformation: a review. Sci. Total Environ. 816, 151574.
Zhang, Y., Tong, M., Yuan, S., Qian, A., Liu, H., 2020. Interplay between iron species transformation and hydroxyl radicals production in soils and sediments during anoxic-oxic cycles. Geoderma 370, 114351.
Zhao, G., Tan, M., Wu, B., Zheng, X., Xiong, R., Chen, B., Kappler, A., Chu, C., 2023. Redox oscillations activate thermodynamically stable iron minerals for enhanced reactive oxygen species production. Environ. Sci. Technol. 57, 8628–8637.
Zhao, G., Wu, B., Zheng, X., Chen, B., Kappler, A., Chu, C., 2022. Tide-triggered production of reactive oxygen species in coastal soils. Environ. Sci. Technol. 56 (16), 11888–11896.
Zhu, T., Lu, X., Liu, H., Li, J., Zhu, X., Lu, J., Wang, R., 2014. Quantitative X-ray photoelectron spectroscopy-based depth profiling of bioleached arsenopyrite surface by Acidithiobacillus ferrooxidans. Geochim. Cosmochim. Acta 127, 120–139.
Zou, J., Qiu, Y.-Y., Li, H., Jiang, F., 2023. Sulfur disproportionation realizes an organic-free sulfidogenic process for sustainable treatment of acid mine drainage. Water Res. 232, 119647.